CHAPTER VI

RESULTS AND DISCUSSION

Experimental results of the experiments described in the preceding chapter are shown in Tables 6.1 and 6.2. In the first serie of experiments, the combustion of nearly all of the fuel mixtures with the fluidizing velocities of $2.6u_{mf}$ was unstable and impossible to operate. In the second serie of experiments, the bed temperatures could not be maintained at the desired value of 850°c if a threshold of oil shale percentage was reached. The bed pressure drop versus ambient gas volume flow rate plots for each fuel mixing ratio of large particle oil shale (2.61mm) are compiled in Figure 6.1 for the determination of minimum fluidizing velocities.The u_{mf} determinations were measured experimentally as no correlations for prediction of u_{mf} of mixtures of different materials were available. The only equation for u_{mf} prediction was developed by Rowe and Nienow[45] to obtain u_{mf} of a mixture of particles of various sizes but all of the same shape and density. However, since the minimum fluidizing velocity of small oil shale (1.44mm) was so low that it could not be determined using the available rotameter. The fluidizing velocities used for small-shale experiments were those assuring the fluidization of the largest particles in the bulk (i.e. lignite) which were about 44 Nm^3/hr.

Table 6.1 First Serie Experimental Results

Ex. No.	O/L	Ca/S	Fuel Feed Rate (kg/hr)	(kcal/hr)	u_{mf}^* (cm/s)	u_{mf}^- (cm/s)	u_o^* (*u_{mf})	u_o^* (m^3/hr)	TAFR (m^3/hr)	EA (%)	(A/F)	Temperature (°c) TIC1	TI2	Tb	TI3	TI4	TI5	TI6	TI7	TI8	TI12
1	0	.925	5.814	17291	34.58	123.50	2.00	44	20.87	110.83	8.68	812	842	827	840	442	268	130	33	81	81
2	0	.925	5.814	17291	34.58	119.12	2.30	51	20.87	144.37	10.07	746	830	788	844	448	283	141	34	88	81
3	0	.925	5.814	17291	34.58	111.37	2.60	57	20.87	173.12	11.25	682	755	719	767	414	271	143	36	85	80
4	.3	1.401	6.517	17291	47.16	167.86	2.00	60	20.60	191.26	10.56	-	823	823	730	540	407	240	39	77	71
5	.3	1.401	6.517	17291	47.16	144.08	2.30	69	20.60	234.95	12.15	-	668	668	684	481	366	219	40	75	64
6	.6	1.782	7.035	17291	47.16	156.18	2.00	60	20.35	194.84	9.79	-	747	747	614	459	331	196	40	63	59
7	.6	1.782	7.035	17291	47.16	149.44	2.30	69	20.35	239.07	11.25	-	703	703	600	445	340	200	41	64	55
8	1	2.185	7.564	17291	53.44	166.57	2.00	68	20.12	237.97	10.32	690	683	687	626	360	240	123	36	75	61
9	1	2.185	7.564	17291	53.44	154.42	2.30	78	20.12	287.67	11.83	610	624	617	574	463	364	215	41	69	50
10	3	3.114	8.904	17291	52.66	163.28	2.00	67	19.54	242.89	8.63	577	786	682	723	407	260	134	35	84	66
11	3	3.114	8.904	17291	52.66	152.17	2.30	77	19.54	294.06	9.92	591	642	617	675	398	268	138	35	87	62
12	7	4.018	9.769	17291	56.59	204.86	2.00	72	19.17	275.59	8.46	825	858	842	785	447	297	156	36	97	87
13	7	4.018	9.769	17291	56.59	181.35	2.30	83	19.17	332.97	9.75	679	748	714	695	423	280	146	36	90	63
14	8	5.194	10.82	17291	56.59	186.86	2.00	72	18.73	284.41	7.64	738	750	744	720	426	295	160	35	92	73
15	8	5.194	10.82	17291	56.59	174.00	2.30	83	18.73	343.14	8.80	655	693	674	707	443	306	160	36	97	63

Ex. No.	Ash (kg/hr)	Fly Ash (kg/hr)	Flue Gas Analysis O_2(%)	CO_2(%)	CO(ppm)	SO_2(ppm)	NO(ppm)	Ash Analysis C(%)	H(%)	N(%)	S(%)	Fly Ash Analysis C(%)	H(%)	N(%)	S(%)	η_c	η_s	Note
1	.354	.266	4.30	16.10	3514	2031	98	44.69	1.07	1.15	4.85	2.11	.46	.14	8.09	93.14	41.56	
2	.378	.272	6.70	14.30	4183	1779	87	40.66	1.13	1.25	4.23	1.60	.46	.09	8.24	93.38	41.29	
3	.27	.519	7.60	12.40	4612	933	64	51.93	1.87	1.66	3.82	1.97	.53	.07	9.80	93.70	65.74	
4	.997	1.431	7.50	11.50	4467	432	11	7.78	.17	.21	1.49	7.52	.18	.14	4.19	91.94	82.86	slag formed
5	1.249	1.584	9.80	9.40	6195	45	34	12.50	.34	.37	1.50	5.17	.18	.15	4.40	89.64	97.95	slag formed
6	.82	1.436	11.30	8.40	4323	299	38	3.64	.13	.11	1.30	6.63	.11	.14	4.65	94.38	87.97	slag formed
7	1.264	1.724	10.90	8.10	5534	100	89	6.33	.18	.20	2.06	8.87	.21	.26	3.36	89.53	95.39	slag formed
8	1.632	.657	11.00	9.20	2597	21	128	2.85	.23	.07	2.24	3.85	.37	.23	7.38	96.67	99.02	
9	2.34	1.857	11.50	7.60	12581	26	287	5.30	.23	.18	1.11	3.95	.14	.26	3.16	90.84	98.61	
10	3.72	.704	10.00	9.80	1764	19	174	1.35	.13	.04	1.44	6.26	.14	.16	3.70	95.23	99.06	
11	1.066	2.095	11.10	8.50	1674	25	193	3.36	.14	.08	1.30	5.05	.17	.16	3.12	92.84	98.59	
12	4.86	.687	8.50	10.60	3262	43	139	.98	.08	.02	1.09	4.30	.14	.14	3.20	95.86	97.60	
13	5.22	.677	10.20	9.40	2165	26	201	1.69	.23	.08	1.05	2.19	.12	.07	3.06	94.47	98.34	
14	5.79	1.293	8.70	10.10	3814	31	273	.65	.10	.02	.72	1.74	.24	.11	2.28	96.51	98.18	
15	6.222	1.148	10.90	8.10	2753	22	158	1.05	.13	.04	.74	2.29	.22	.14	2.21	94.68	98.52	

d_p oil shale = 2.61 mm d_p lignite = 2.59 mm *inlet gas condition TAFR = theoretical air flow rate EA = excess air

-in-bed condition calculated by gas law

Table 6.2 Second Serie Experimental Results

Ex. No.	O/L	Ca/S	Fuel Feed Rate (kg/hr)	(kcal/hr)	u_{mf} (cm/s)	u_{mf}^* (cm/s)	($*u_{mf}$)	u_o^* (m^3/hr)	TAFR (m^3/hr)	EA (%)	(A/F)	Temperature (°C) T1C1	T12	Tb	T13	T14	T15	T16	T17	T18	T112
16	0	.925	12.076	35914	34.58	123.72	3.27	72	43.35	66.09	6.84	804	854	829	875	639	493	320	42	86	81
17	1	2.185	10.77	24620	53.44	196.06	2.12	72	28.65	151.31	7.67	854	859	857	781	446	289	159	36	94	64
18	3	3.114	13.994	27175	52.66	186.19	2.15	72	30.72	134.36	5.90	823	808	816	719	425	266	146	36	86	90
11	7	4.018	9.769	17291	56.59	204.86	2.00	72	19.17	275.59	8.46	825	858	842	785	447	297	156	36	97	87
1	0	.925	5.814	17291	34.58	123.50	2.00	44	20.87	110.83	8.68	812	842	827	840	442	268	130	33	81	81
19	.5	1.664	6.098	15339	n.d.	—	—	44	18.11	142.96	8.28	792	874	833	789	540	389	227	37	69	71
20	1	2.185	6.18	14127	n.d.	—	—	44	16.44	167.64	8.17	851	831	841	730	370	227	112	36	74	59
21	3	3.114	12.99	25226	n.d.	—	—	44	28.51	54.33	3.89	854	860	857	830	417	242	124	34	80	68
22	7	4.018	20.424	36150	n.d.	—	—	44	40.08	9.78	2.47	773	782	778	767	399	246	127	35	81	90
23	7	5.194	30.252	48344	56.59	178.59	2.00	72	52.36	37.51	2.73	688	710	699	732	445	294	162	37	90	70
24	7	5.194	10.82	17291	<28.29	—	—	25	18.73	33.48	2.65	646	655	651	604	246	153	74	34	57	69
25	7	5.194	10.82	17291	<28.29	—	—	30	18.73	60.17	3.18	657	671	664	642	312	175	85	34	63	80
26	7	5.194	10.82	17291	<28.29	—	—	35	18.73	86.87	3.71	664	676	670	643	414	305	165	36	57	73

- freeboard water rate = 4 l/min

Ex. No.	Ash (kg/hr)	Fly Ash (kg/hr)	Flue Gas Analysis O_2(%)	CO_2(%)	CO(ppm)	SO_2(ppm)	NO(ppm)	Ash Analysis C(%)	H(%)	N(%)	S(%)	Fly Ash Analysis C(%)	H(%)	N(%)	S(%)	η_c	η_s	Note
16	1.602	1.185*	flue gas temperature was too high to collect the sample					55.54	.93	1.46	2.82	25.61	.20	.59	3.91	75.93	47.36	*measured value
17	3.264	1.229	7.00	13.40	5186	424	174	2.40	.11	.02	1.94	6.72	.15	.21	3.30	94.76	84.97	
18	5.484	.871	6.10	14.30	3708	30	218	1.36	.10	.09	1.14	3.74	.40	.34	7.17	96.55	98.97	
11	4.86	.687	8.50	10.60	3262	43	139	.98	.08	.02	1.09	4.30	.14	.14	3.20	95.86	97.60	
1	.354	.266	4.30	16.10	3514	2031	98	44.69	1.07	1.15	4.85	2.11	.46	.14	8.09	93.14	41.56	
19	.889	.25	4.60	14.30	4183	2332	193	6.18	.12	.11	.46	12.55	.16	.28	5.09	95.67	21.38	slag formed
20	1.74	.664	7.60	12.60	4044	468	267	1.85	.12	.05	.85	4.36	.55	.28	6.48	96.53	82.39	
21	6.606	.29	1.40	18.60	>12101	3000	1817	1.13	.05	.05	.34	3.83	.39	.25	4.73	97.03	30.88	
22	11.106	1.227	.50	20.50	>12101	1146	7557	1.36	.07	.03	.82	5.58	.21	.19	3.13	94.36	80.63	
23	19.884	4.26	4.10	16.50	10718	43	988	1.66	.13	.03	.56	4.01	.19	.17	2.10	89.61	99.07	
24	7.77	0	1.80	16.20	>12101	329	3388	2.67	.13	.08	.85	6.31	.47	.31	3.96	87.96	91.10	
25	7.71	0	3.40	15.20	>12101	153	2189	2.93	.11	.05	.94	5.25	.36	.25	2.15	86.89	99.97	
26	7.62	.4	4.40	14.60	>12101	108	2391	1.74	.09	.07	.82	3.61	.21	.19	1.93	91.47	96.84	

d_p lignite = 2.59mm * inlet gas condition TAFR = theoretical air flow rate EA = excess air n.d.= not determined

*in-bed condition *d_p oil shale = 1.44mm

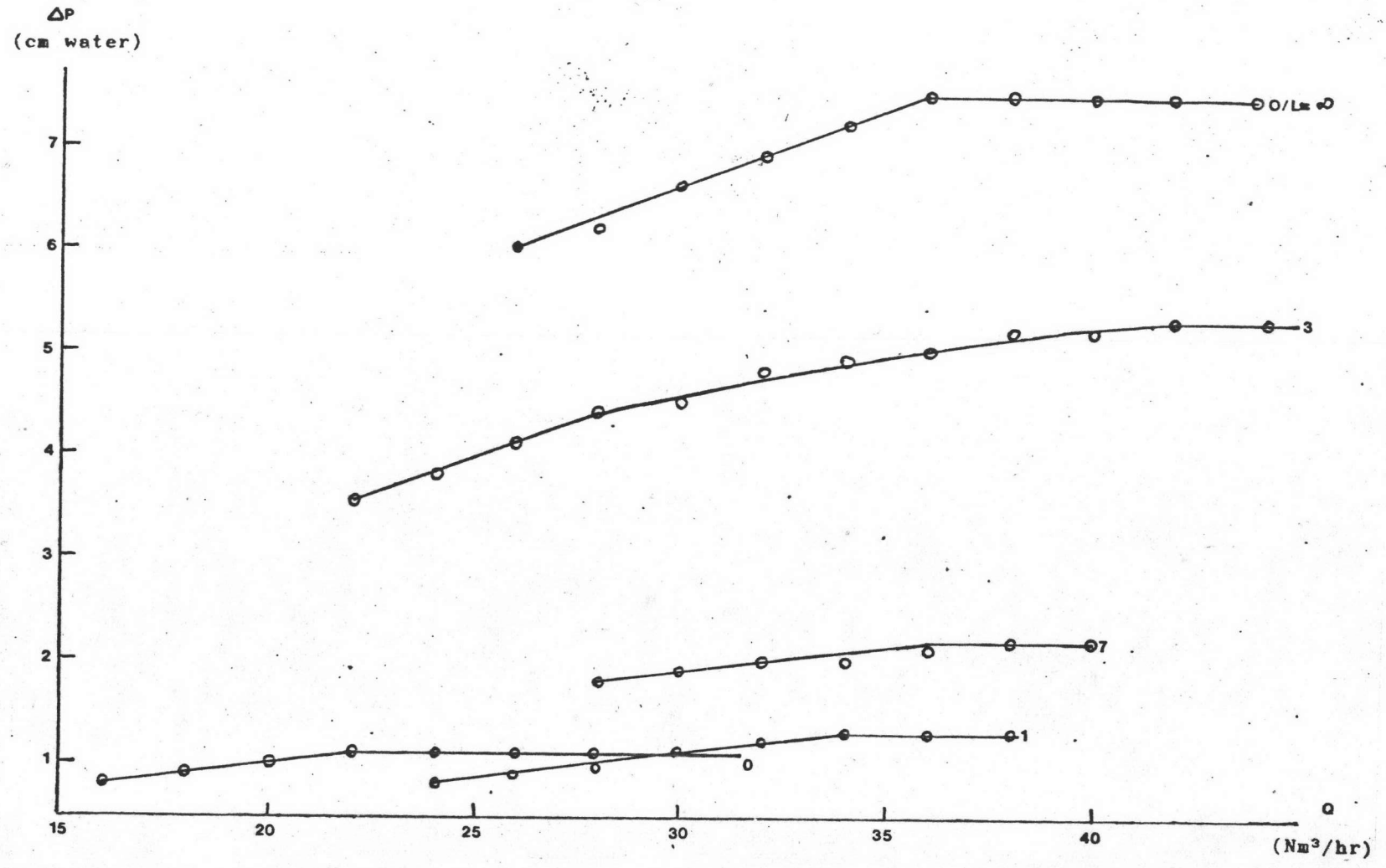

Figure 6.1 Bed Pressure Drop Versus Volumetric Flow Rate Plots for Various Oil Shale to Lignite Weight Ratios

A damper problem encountered in running the combustor was caused by moisture both from fuel feeds and combustion reaction. A portion of moisture was condensed in the cyclones, this moisture entrapped fly ash and, then, adhered to the cylinder wall. This made elutriation-rate measurement inaccurate or, in some cases, impossible. Nevertheless, the graph of cyclones efficiency is provided in Appendix E herewith. Accordingly, the elutriation rates compiled in Table 6.1 and 6.2 were calculated from sulfur balances for which an example of calculation is provided in Appendix D. Furthermore, in experiments using lignite dominated fuel mixtures the moisture problem became more serious. This was so because at least a part of moisture evolved from vaporization and combustion went through the gravity drop pipe of the screw feeder and condensed mostly at the upper end connected to the screw housing. The condensed water caused the fuel fines, produced by the mechanical movement in the screw feeder, adjacent to that area become a thick slurry, and clogged the fuel passage eventually. Thus, this mentioned part was removed for cleaning before hand and the experiments had been completed before the blockage would occur.

Referring again to Tables 6.1 and 6.2, the theoretical air flow rate calculations can be readily performed using stoichiometric air data represented in Table 5.1, fuel mixing ratios and fuel feed rates. The excess air defined as the quantity of air used beyond the theoretical air and air to fuel mass ratio are also compiled in these Tables. The "slag formed" term, as noted in these Tables, indicates slag formation in the vicinity of the internal bed wall during the start up process, i.e.

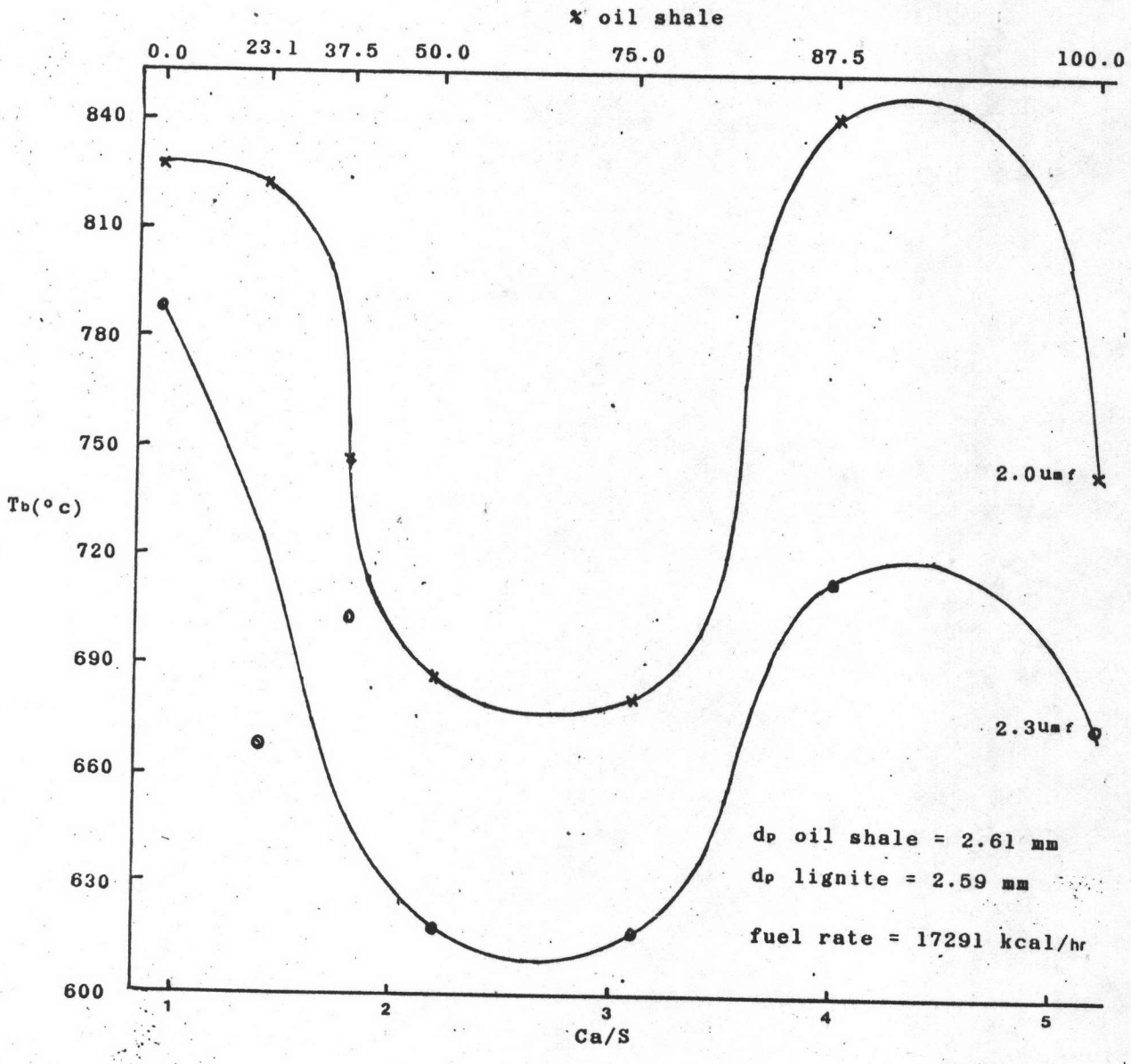

Figure 6.2 The Effect of Percent Oil Shale or Calcium to Sulfur Mole Ratio on Bed Temperature

the introduction of fluidizing air was too slow to blow the ignited particles away from the preheated refractory wall prior to the ash fusion. The fused particles blocked the TIC1 thermocouple (see Figure 5.1) but did not alter the combustion performance.

The bed temperature attained with the combustion of 2.61 mm oil shale and 2.59 mm lignite mixtures at equivalent feed rate of 17,291 kcal/hr, and fluidizing velocities of 2.0 and 2.3 times of the individual minimum fluidizing velocity, were plotted versus calcium to sulfur mole ratio of the fuel mixtures and shown in Figure 6.2. Moving from the right most of the curves, which is the bed temperatures of pure oil shale combustions, to the left it can be noticed that addition of a little fraction of lignite into oil shale feed caused the bed temperature to increase. The higher fraction of lignite (Ca/S below about 4.3) caused the bed temperature to decrease. As the lignite fraction in fuel mixture increased further, the bed temperature started to increase again (Ca/S below about 2.7). This may be caused by the lower air flow rate used which results in lower heat convection along with the flue gas. However, the bed temperature variations as O/L changed may be affected by non-uniform fuel properties.

The carbon combustion efficiency (n_c) and desulfurization efficiency (n_s) are defined as

$$n_c = 1 - \frac{\text{carbon output}}{\text{carbon input}} \qquad (6.1)$$

$$n_s = \frac{\text{sulfur output}}{\text{sulfur input}} \qquad (6.2)$$

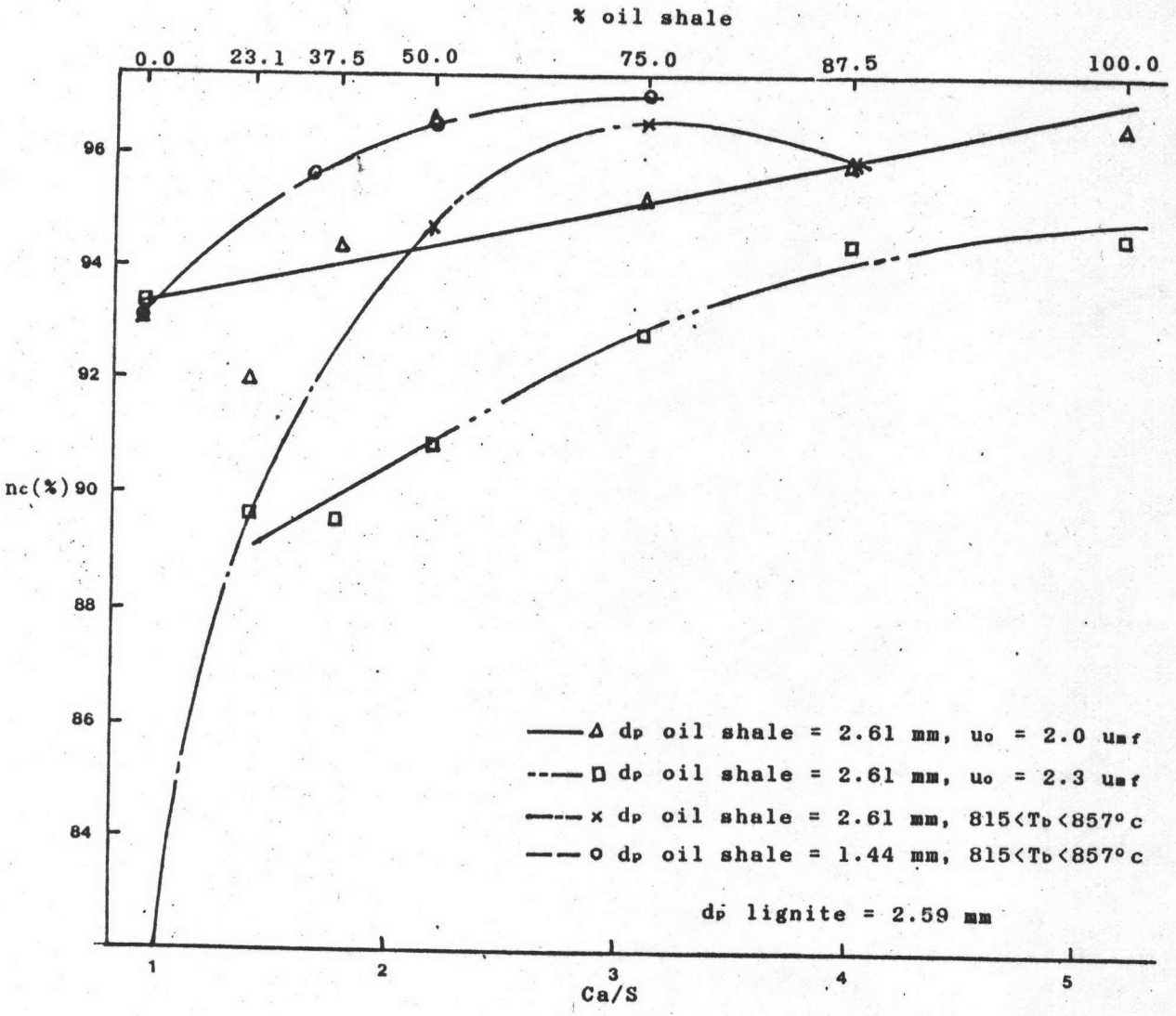

Figure 6.3 The Effect of Percent Oil Shale or Calcium to Sulfur Mole Ratio on Carbon Combustion Efficiency

Results from these calculations were plotted versus Ca/S ratio and shown respectively in Figures 6.3 and 6.4. Moreover, carbon monoxide, sulfur dioxide, and nitric oxide emissions in terms of pounds per million Btu are depicted in Figures 6.5, 6.7, and 6.8 respectively.

In Figure 6.3, carbon combustion efficiencies of 2.61 mm oil shale and 2.59 mm lignite mixtures at an equivalent fuel feed of 17,291 kcal/hr, and fluidizing velocities of 2.0 and 2.3 times of the corresponding minimum fluidizing velocity, were plotted versus calcium to sulfur mole ratio of the fuel mixtures. It can be seen that combustion efficiency increases with calcium to sulfur mole ratio or, in other words, with oil shale to lignite weight ratio. For the lignite burned in the bed, coal debris from attrition and ash from combustion are found to strip off after their formation at the coal surface, and elutriated as fly ash resulting in shrinkage in particle size and carbon loss in the fly ash. The oil shale, on the other hand, are observed to retain the same particle size during combustion in the bed, which is an indication for relatively low attrition rate. Accordingly, as calcium to sulfur mole ratio increases with, in turn, the lignite fraction in fuel feed mixture decreasing, carbon loss along with fly ash decreases which causes the combustion efficiency to increase. Furthermore, it was found that carbon combustion efficiency decreases as fluidizing velocity increases. This is because the higher gas velocity causes elutriation rate higher and more heat convection by the fluidizing gas which, in turn, causes the bed temperature lower and, then, lower combustion rate. These phenomena result in more carbon loss in both fly ash and

drained ash.

Also in Figure 6.3, carbon combustion efficiencies of 1.44 mm oil shale and 2.59 mm lignite mixtures and of 2.61 mm oil shale and 2.59 mm lignite mixtures at fuel feed rates for maintaining the bed temperature around 850°c (between 815°c to 857°c in the experiments) and fluidizing velocities of 2.0 times of the minimum fluidizing velocities of the largest particles in the mixtures, were plotted versus calcium to sulfur mole ratio of the fuel mixtures. It can be noticed that combustion of small-shale mixtures were more complete than of the big-shale mixtures. This is because larger surface area per unit volume of smaller shale results in higher reaction rates which causes the smaller shale to combust to more degree of completion than the bigger one before it comes out the firebox. Another relevant factor is the difference of fluidizing gas velocities. Moreover, the combustion efficiency increases with Ca/S until the ratio of about 3 is reached and, then, it becomes constant or even lower. Accordingly, the optimum calcium to sulfur mole ratio, in case of the bed temperature was kept around 850°c ,was about 3, which is equivalent to oil shale to lignite weight ratio of about 3. The obtained carbon combustion efficiencies were compared to those available from prior investigators in Appendix F.

In Figure 6.4, desulfurization efficiencies of 2.61 mm oil shale and 2.59 mm lignite mixtures at an equivalent fuel feed rate of 17,291 kcal/hr, and fluidizing velocities of 2.0 and 2.3 times of the individual minimum fluidizing velocity, were plotted versus calcium to sulfur mole ratio of the fuel mixtures. From reactions[37]

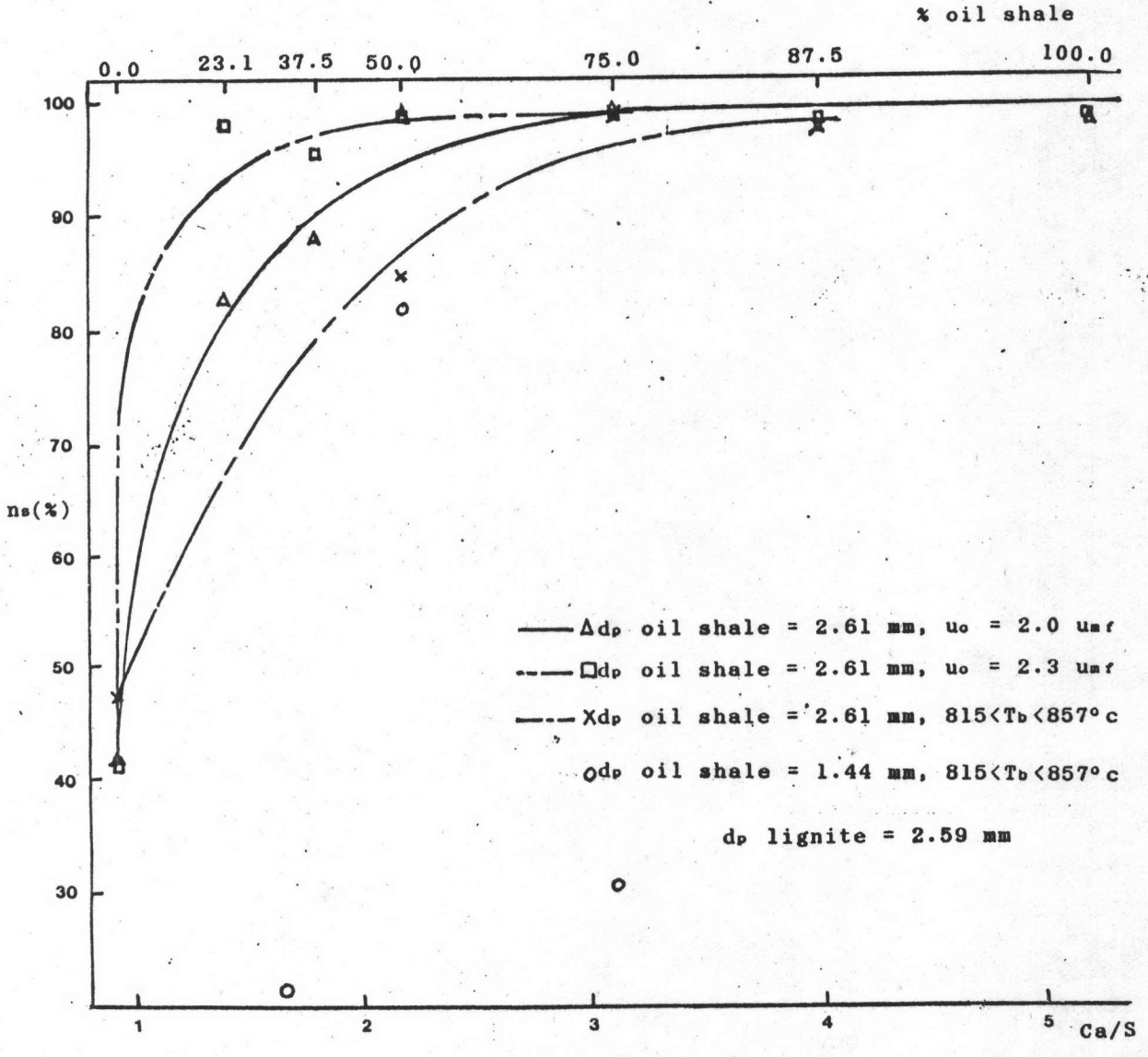

Figure 6.4 The Effect of Percent Oil Shale or Calcium to Sulfur Mole Ratio on Desulfurization Efficiency

$$CaCO_3 \xrightarrow{>770^\circ c} CaO + CO_2 \qquad (6.3)$$

calcination of calcium carbonate

$$2CaO + 2SO_2 + O_2 \longrightarrow 2CaSO_4 \qquad (6.4)$$

sulfation of fully calcined calcium carbonate

$$CaCO_3 + SO_2 + 1/2O_2 \xrightarrow{<770^\circ c} CaSO_4 + CO_2 \qquad (6.5)$$

sulfation of raw calcium carbonate

$$CaSO_4 + CO \xrightarrow{>1100^\circ c} CaO + CO_2 + SO_2 \qquad (6.6)$$

thermal decrepitation

reaction 6.6 can be ignored because the bed temperatures did not exceed even 900°c. Examining these reactions leads to the fact that desulfurization in an FBC depends on bed calcium content and excess oxygen in the emulsion phase. In Figure 6.4, desulfurization efficiency increases rapidly at the range of low calcium to sulfur mole ratios. This may be explained as follows:

In case of lignite-dominant mixtures burning without other bed materials, the low ash content and high attrition rate of lignite causes large bed voidage, i.e. lean phase fluidization, which results in good solid-gas contact. Subsequently, although the bed calcium content is low, its utilization is quite efficient. This causes desulfurization efficiency to increas quickly as the bed calcium content increased.

After these initial Ca/S values, say beyond 1.0, the bed becomes denser which may cause the gas to form bubbles, the extent of gas by-passing via the bubbles

increases with oil shale fraction in the fuel mixtures. Moreover, sulfur dioxide being generated by the fuel combustion would has a higher fraction in the bubbles. These are reasons why desulfurization efficiency increases more slowly as the Ca/S increases. Furthermore, while the fluidizing gas is increased at the same Ca/S, thereby increasing the excess oxygen as can be observed in Figure 6.4, the desulfurization efficiency becomes better. This phenomenon confirms the above assumptions to some extent. Subsequently, the more excess air is used, the more efficient is the utilization. This statement can be verified by the calcium to sulfur mole ratio which is decreased from about 3.0 for $u_o = 2.0u_{mf}$ curve to about 2.0 for $u_o = 2.3u_{mf}$ curve before these curves levell off. The levelled off section of the curves appear to have the same manner. This may be because of excess calcium and oxygen.

Also in Figure 6.4, desulfurization efficiencies of 1.44 mm oil shale and 2.59 mm lignite mixtures and of 2.61 mm oil shale and 2.59 mm mixtures at fuel feed rates for maintaining the bed temperature around 850°c, and fluidizing velocities of 2.0 times the minimum fluidizing velocities of the largest particles in the mixtures, were plotted versus calcium to sulfur mole ratios of the fuel mixtures. The curve of big-shale mixtures has lower slope at low Ca/S than the former curves in Figure 6.4 and the calcium to sulfur mole ratio where the curve starts to be levelled off is shifted to about 3.5. This is because of higher fuel feed rates needed for raising the bed temperature to the desired level, causing the excess oxygen to decrease as shown in Tables 6.1 and 6.2. For small-shale mixtures, the plots are substantially scattered. This may be caused by

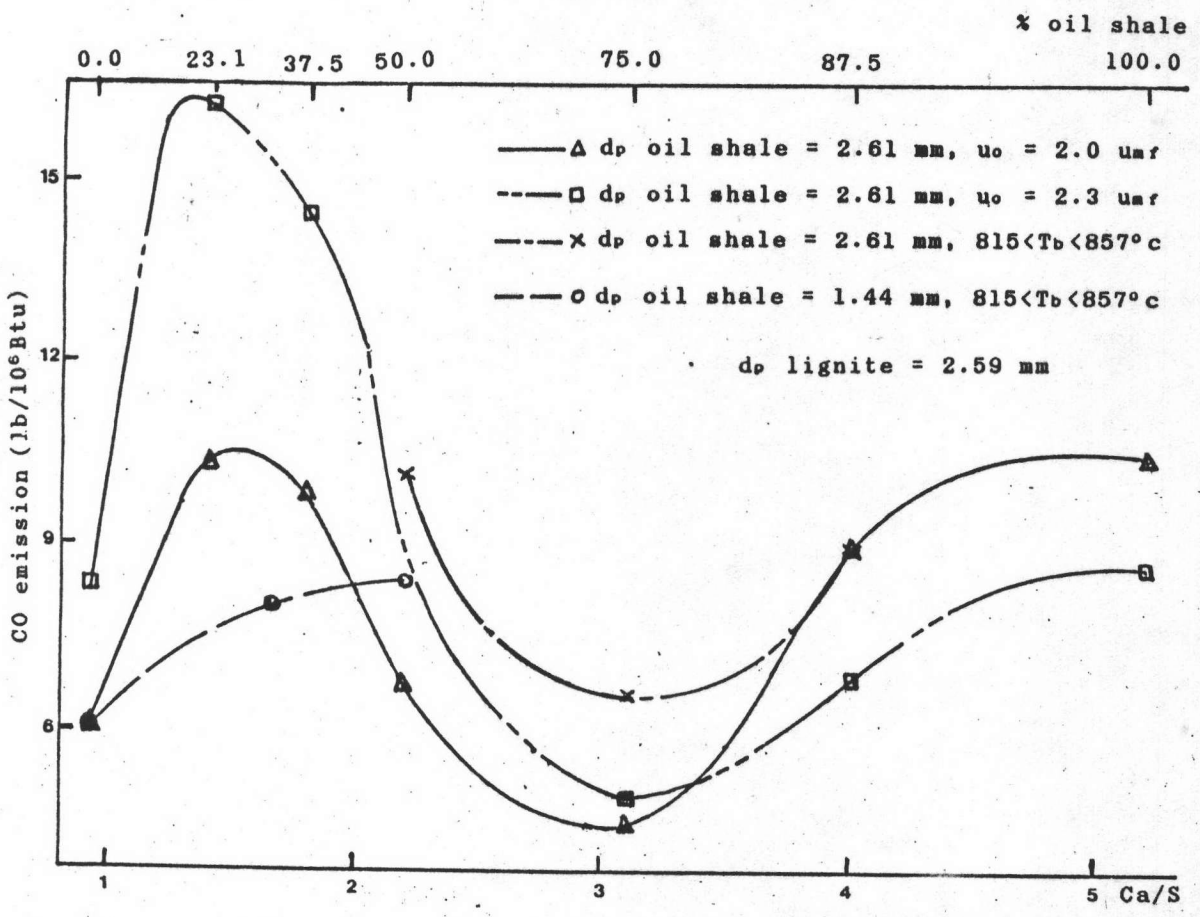

Figure 6.5 Carbon Monoxide Emissions of Various Experimental Conditions

the smaller bed voidage than in case of combustion with big shale mixtures in which promoting the fluidizing air to by-pass easier through the bed in form of bubbles, and different fuel feed rates needed for raising the bed temperature to the desired value, causing variation in the excess oxygen among the tests.

Carbon monoxide emissions as a function of calcium to sulfur mole ratio of various experimental conditions are shown in Figure 6.5. Prior investigators[38] have found that at relatively low operating temperature of FBCs there is potential for unacceptably high emission of CO. Rapid increases in emissions from small scale FBCs have been observed when the bed temperature has been reduced, with the reported transition temperature varying in the range of 950 to 1050K (677 to 777°c). The bed temperatures below this range may not be so efficient enough for combustion of carbon monoxide diffusing away from the solid-fuel surface and allows it to join with the main gas stream. Moreover, CO may be produced by elutriated fines burning in the freeboard. CO produced at the surface of fines quickly diffuses away from the particles, it can escape the vicinity of the particle unreacted. Since the freeboard is usually deficient in oxygen and lower in local temperature, the CO oxidation there would be slow[39].

To verify the effect of bed temperature and fly ash on the CO emission, weights of carbon monoxide emitted per million Btu were plotted as a function of elutriated carbon in the same basis at various bed temperatures in Figure 6.6. In this Figure, there seems to be no relationship between carbon monoxide and bed temperature whereas the

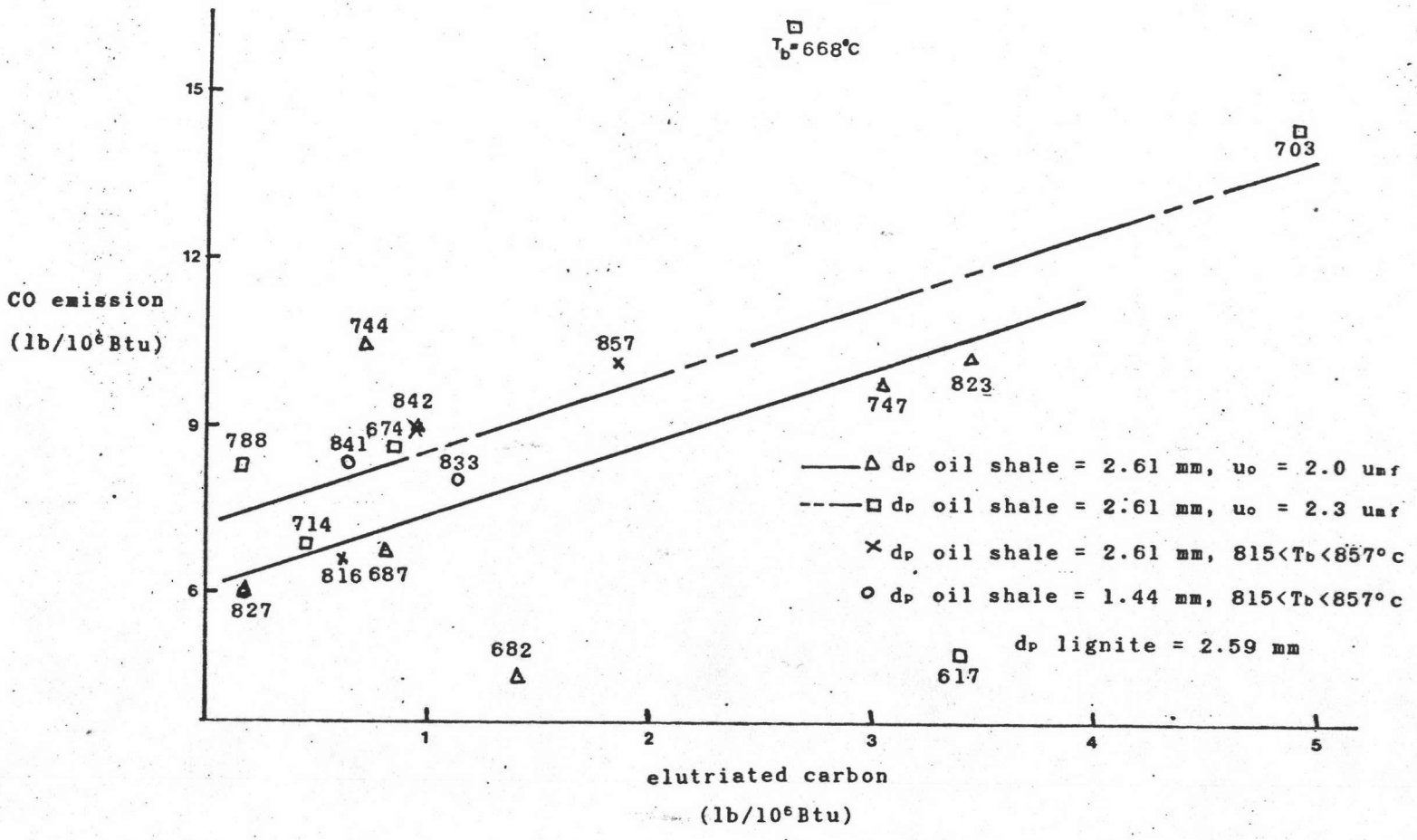

Figure 6.6 Effect of Elutriated Carbon and Bed Temperature on Carbon Monoxide Emission

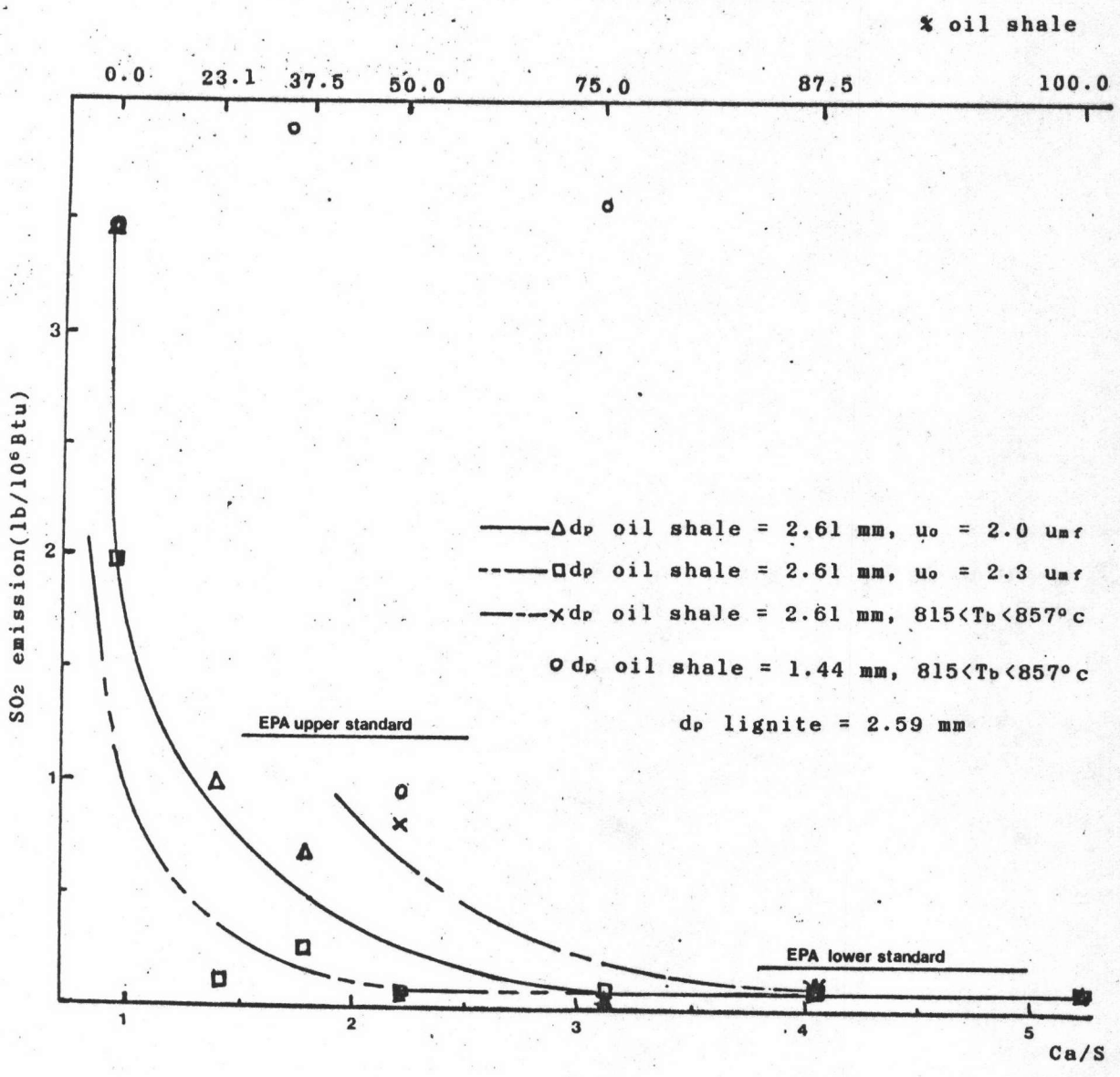

Figure 6.7 Sulfur Dioxide Emissions of Various Experimental Conditions

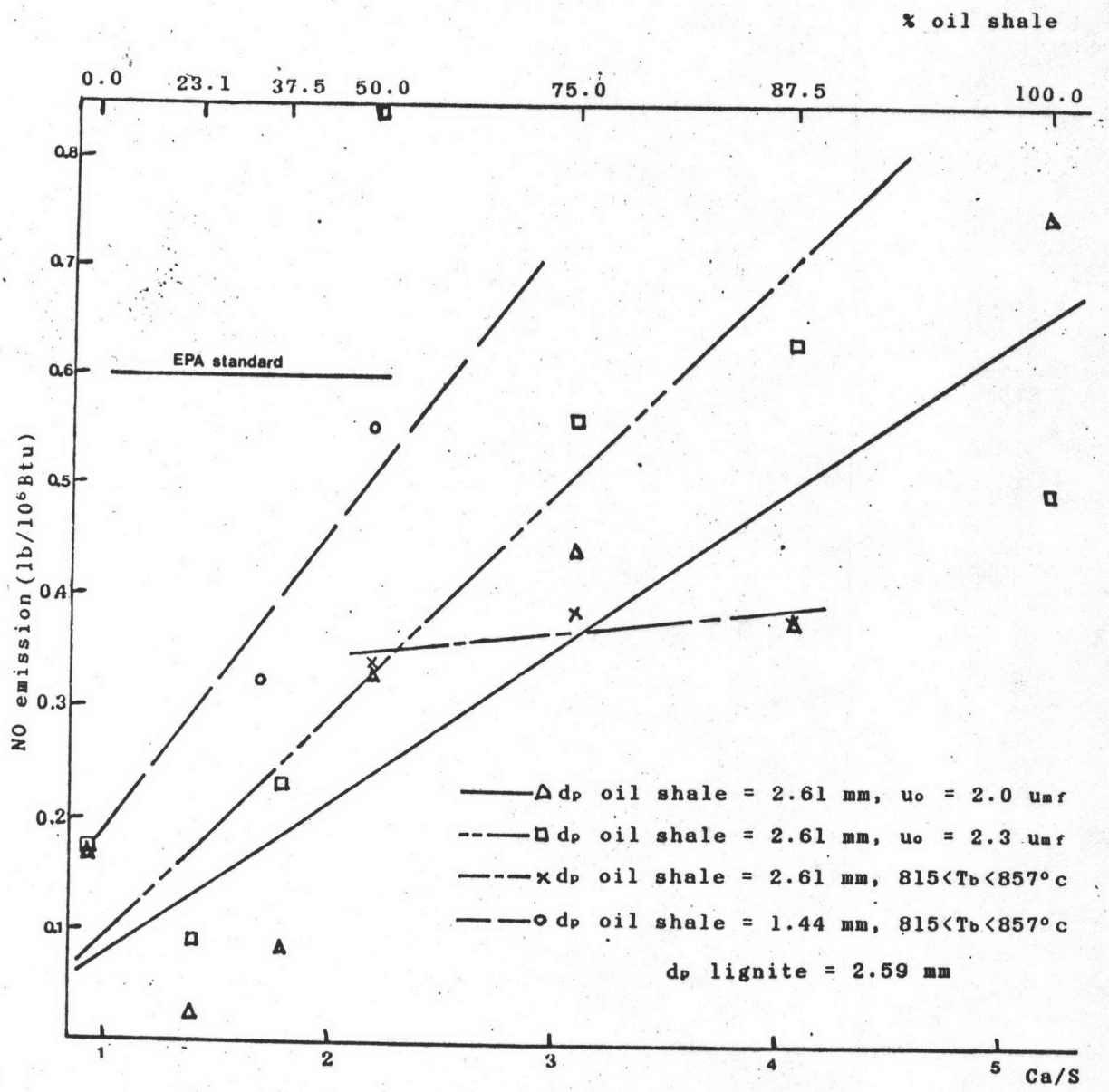

Figure 6.8 Nitric Oxide Emissions of Various Experimental Conditions

emission has a tendency to increase along with the elutriated carbon, even though the plots are relatively scattered.

The graphs of sulfur dioxide emission versus fuel calcium to sulfur mole ratio of various experimental condition are shown in Figure 6.7. It can be stated that this Figure is the "reverse" of Figure 6.4 and the explanation will be similar to that made for that Figure.

Dealing with nitric oxide, its emissions at various experimental conditions were plotted versus calcium to sulfur mole ratio of fuel feeds as shown in Figure 6.8. It may be noticed that NO emission increases with the Ca/S in every set of experiments although the nitrogen content in oil shale is much lower than that in lignite (see Table 5.1). This circumstance results in an opposition between NO emission and fuel nitrogen content, i.e. higher emission at lower nitrogen content. The following explanation will be made to clear the puzzling event.

The oxides of nitrogen, which are known toxicants, originate fron nitrogen compounds in fuels, known as fuel-bond nitrogen which is assumed to be ammonia (NH_3), and from nitrogen in the air. The bed temperature in an FBC is not high enough to burn the atmospheric nitrogen into nitric oxides. Subsequently, the nitrogen oxides are mostly formed from fuel-bond nitrogen. The mechanics of the formation and destruction of nitrogen oxides inside an FBC, as presently known, are as follows:[14,38,40,41,42]

- Decomposition of nitrogen compounds in fuel into volatile nitrogen compounds such as various amines and ammonia.

- Oxidation of decomposed nitrogen compounds to oxides of nitrogen in a high temperature and oxygen-rich zone near the distributor

$$NH_3 + O_2 \xrightarrow{k_1} NO \qquad (6.7)$$

$k_1 = 2.544 * 10^3 T \exp(-15{,}098/T)$ $cm^3/mole*s$

and more NO is formed during the combustion of the residual char.

$$\text{char nitrogen} + O_2 \longrightarrow NO \qquad (6.8)$$

Nitric oxide is the candidate of nitrogen oxides in equation 6.7 and 6.8 because it is considered to be the only oxide of nitrogen existing at the operating temperature of the combustor as shown in the reactions:

$$2N_2O \xrightarrow{500\text{-}900^\circ C} 2N_2 + O_2 \qquad (6.9)$$

$$2N_2O_5 \xrightarrow{50^\circ C} 4NO_2 + O_2 \qquad (6.10)$$

$$N_2O_4 \underset{}{\overset{140^\circ C}{\rightleftharpoons}} 2NO_2 \overset{620^\circ C}{\rightleftharpoons} 2NO + O_2 \qquad (6.11)$$

- "Relaxation" (the return of nitrogen oxides to their equilibrium concentration) and reduction of the oxides of nitrogen back to molecular nitrogen and oxygen under reducing conditions. Relaxation takes place in-bed and/or over-bed. Reduction is effected by the presence of carbon particles and possibly carbon monoxide with sufficient gas residence time.

$$C + NO \longrightarrow 1/2N_2 + CO \qquad (6.12)$$

$$C + 2NO \longrightarrow N_2 + CO_2 \qquad (6.13)$$

$$C + 2NO \longrightarrow N_2O + CO \qquad (6.14)$$

$$CO + NO \longrightarrow 1/2N_2 + CO_2 \qquad (6.15)$$

N_2 and CO_2 were produced in the low temperature region

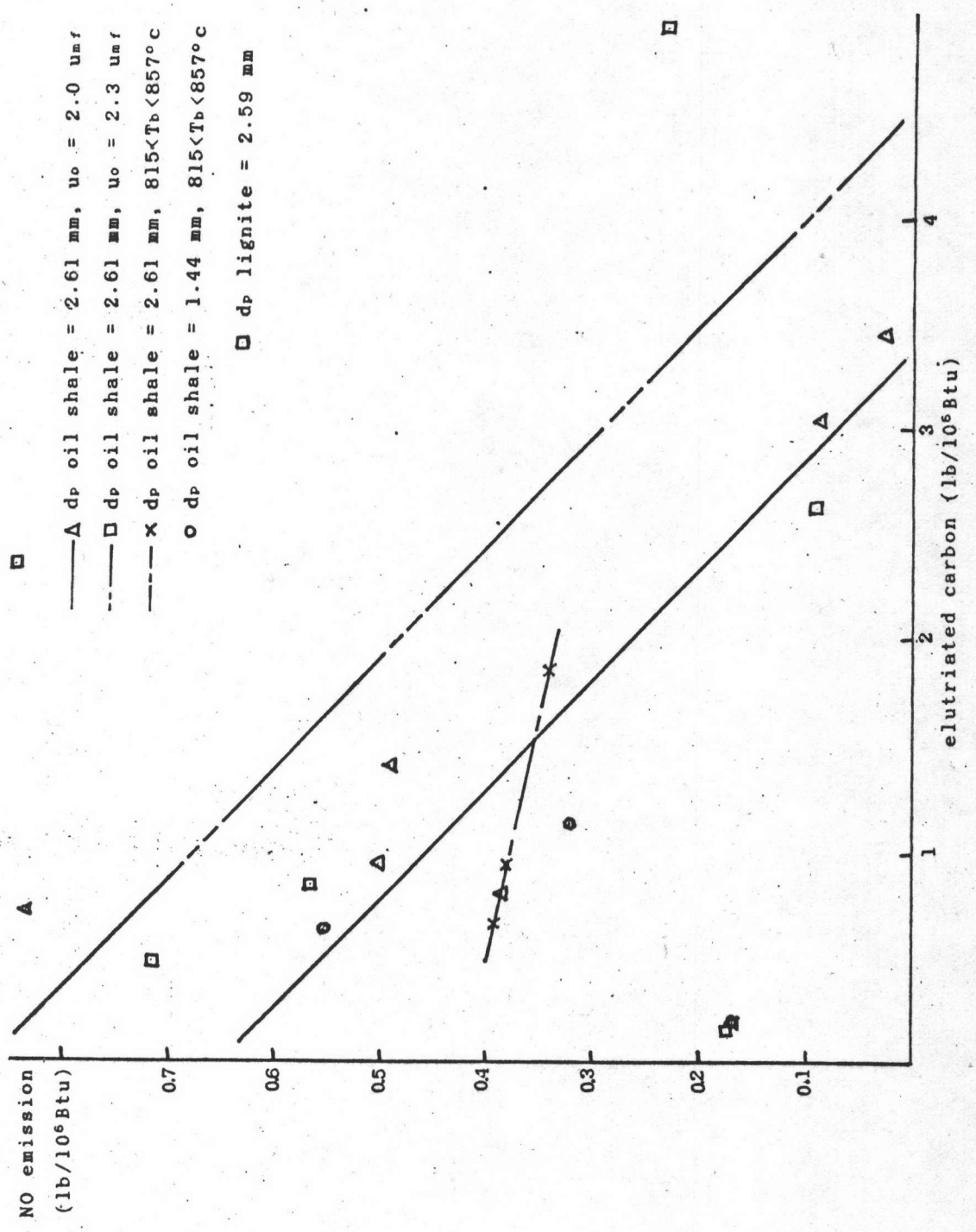

Figure 6.9 Effect of Elutriated Carbon on Nitric Oxide Emission

(<640°c). Equation 6.15 is extremely slow within this region and hence can be disregarded. Thus, equation 6.13 can be regarded as the main reaction occurring. At 680°c and above, equations 6.12 and 6.13 represent the actual reactions that occurring, from which N_2, CO, and CO_2 were formed. As the temperature was raised, the amount of CO_2 that was formed decreased, while the proportion of CO in the reaction products increased.

Furthermore, the NO formed may react with nitrogen containing volatiles in the fluidized combustion temperature range (700-900°c), in the presence of oxygen.

$$NH_3 + NO \xrightarrow{k_2} N_2 \qquad (6.16)$$

$$k_2 = 6.564 * 10^{11}\sqrt{T}\exp(-13{,}588/T) \quad cm^3/mole*s$$

It may be noticed from the above discussion that nitric oxide-carbon reaction has a major role on the reduction of NO emission from the combustor. Accordingly, if carbon concentration in the bed and/or in the freeboard is high nitric oxide emission should be low, as illustrated in Figure 6.9. This is the reason explaining the trends in Figure 6.8.